Novel Keeling plot based methods to estimate the isotopic composition of ambient water vapor

Yusen Yuan[a,b], Taisheng Du[a]*, Honglang Wang[c], Lixin Wang[b]*

[a] Center for Agricultural Water Research in China, China Agricultural University, Beijing 100083, China

[b] Department of Earth Sciences, Indiana University-Purdue University Indianapolis, Indianapolis, Indiana 46202, USA

[c] Department of Mathematical Sciences, Indiana University-Purdue University Indianapolis, Indianapolis, Indiana 46202, USA

* Corresponding author: Dr. Taisheng Du
Fax: +86-10-62737611; Tel: +86-10-62738398
Email: dutaisheng@cau.edu.cn

* Corresponding author: Dr. Lixin Wang
Fax: +1-1-317-274-7966; Tel: +1-317-274-7764
Email: lxwang@iupui.edu

Highlights:

1. Two new methods were developed to estimate the isotopic composition of ambient vapor.
2. Theoretical derivations were provided for these two methods.
3. Linear regression showed strong agreement between the two methods.
4. The methods provide a possibility to calculate the proportion of evapotranspiration fluxes to total atmospheric vapor using the same instrumental setup for the traditional Keeling plot investigations.

Abstract

Keeling plot approach, a general method to identify the isotopic composition of source atmospheric CO_2 and water vapor (i.e., evapotranspiration), has been widely used in terrestrial ecosystems. The isotopic composition of ambient water vapor (δ_a), an important source of atmospheric water vapor, is not able to be estimated to date using the Keeling plot approach. Here we proposed two new methods to estimate δ_a using the Keeling plots: one using intersection point method and another relying on the Intermediate Value Theorem. As actual δ_a value was difficult to measure directly, we used two indirect approaches to validate our new methods. First, we made an external vapor tracking using Hybrid Single Particle Lagrangian Integrated Trajectory (HYSPLIT) model to facilitate explaining the variation of δ_a. The trajectory vapor origin results were consistent with the expectations of the δ_a values estimated by these two methods. Second, regression analysis was used to evaluate the relationship between δ_a values estimated from these two independent methods and they are in strong agreement. This study provides an analytical framework to estimate δ_a using existing facilities, and provides important insights into the traditional Keeling plot approach by showing: a) a possibility to calculate the proportion of evapotranspiration fluxes to total atmospheric vapor using the same instrumental setup for the traditional Keeling plot investigations, and b) perspectives on estimation of isotope composition of ambient CO_2 ($\delta_a{}^{13}C$).

Key words: HYSPLIT, intersection point, Intermediate Value Theorem, Keeling plot, stable isotope

1. Introduction

Stable isotopes of hydrogen and oxygen ($^1H^2HO$ and $H_2{}^{18}O$) have been widely used in root water uptake source identification (Corneo et al., 2018, Mahindawansha et al., 2018, Lanning et al., 2020) and evapotranspiration (ET) partitioning (Brunel et al., 1997; Wang et al., 2010; Cui et al., 2020) in terrestrial ecosystems based on Craig-Gordon model (Craig and Gordon, 1965), isotope mass balance and mechanisms of isotopic fractionation (Majoube, 1971; Merlivat and Jouzel, 1979). With the advent of laser isotope spectrometry capable of high frequency (1 Hz) measurements of the isotopic composition of atmospheric water vapor (δ_v) and atmospheric water vapor content (C_v) (Kerstel and Gianfrani, 2008; Wang et al., 2009), the number of studies based on high frequency ground-level isotope measurements was continuously increasing. These studies generate new insights into the processes that affect δ_v, including meteorological factors (Galewsky et al., 2011; Steen-Larsen et al., 2013), biotic factors (Wang et al., 2010) and multiple factors (Parkes et al., 2016). Such increase in δ_v measurements allows an isotope-enabled global circulation models (Iso-GCMs) to estimate the variation of water vapor isotope parameters at a global scale (Werner et al., 2011). Concomitantly, more than δ_v, several new methods using high frequency ground-level isotope measurements were devised to directly estimate the isotopic composition of leaf water (Song et al., 2015) and leaf transpired vapor (Wang et al., 2012).

Evapotranspiration is a crucial component of water budget across scales such as field (Wagle et al., 2020), watershed (Zhang et al., 2001), regional (Hobbins et al., 2001) and global (Jung et al., 2010) scales. The water isotopic composition of ET (δ_{ET}) was generally estimated by Keeling plot approach (Keeling, 1958). It was first used to explain carbon isotope ratios of atmosphere CO_2 and to identify the sources that contribute to increases in atmospheric CO_2 concentration, and has been further used to estimate δ_{ET} in recent two decades (Yakir and Sternberg, 2000). Keeling plot analyses can be applied using δ_v and C_v output by laser based analyzer either from different heights (Yepez et al., 2003; Zhang et al., 2011; Good et al., 2012) or at one height with continuous observations (Wei et al., 2015; Keppler et al., 2016). Although the intercept of the linear regression line was commonly used as estimated δ_{ET}, the slope of the Keeling plot was also used to estimate δ_{ET} by re-arranging the Keeling plot equations (Miller and Tans, 2003; Fiorella et al., 2018). Keeling plot approach was based on isotope mass balance and two-source assumption using two equations with three unknowns. As a result, the isotopic composition of other potential sources (e.g., water vapor not from ET), as well as isotopic composition of ambient water vapor (δ_a), were not able to be estimated directly using the Keeling plot approach. That is one of the reasons why field scale moisture recycling is difficult to estimate to date.

In this study, we proposed two new methods to estimate δ_a, one based on the intersection of two Keeling plots of two continuous observation moments and the other based on the Intermediate Value Theorem. Proposition and proof were provided, and the new methods were tested using field observations. As direct observations of δ_a rarely exist (Griffis et al., 2016), we tested our methods by (a) making an external water vapor tracking investigation according to HYSPLIT model to explain the variation of estimated δ_a, and (b) making a regression analysis on daily scale and point to point scale using δ_a estimated by these two independent methods.

2. Materials and Methods

2.1 Theory

The atmospheric vapor concentration in an ecosystem reflects the combination of ambient vapor that is already exist in the atmosphere and the vapor that is added through evaporation (E) and transpiration (T) (Yakir and Sternberg, 2000). Keeling plot approach is based on the combination of a bulk water mass balance equation and an isotope mass balance equation:

$$C_v = C_a + C_{ET} \quad , \quad (1)$$

$$C_v\delta_v = C_a\delta_a + C_{ET}\delta_{ET} \quad , \quad (2)$$

where δ_a, δ_{ET} and δ_v are isotope composition of ambient water vapor, ET, and atmospheric water vapor, respectively, and C_a, C_{ET} and C_v are the corresponding concentrations of water vapor. Note that all quantities here are time dependent, and δ_v and C_v also depend on heights.

Combining Eq. (1) and Eq. (2), we have the following traditional linear Keeling plot relationship between δ_v and $1/C_v$ with intercept δ_{ET} and slope $C_a(\delta_a - \delta_{ET})$,

$$\delta_v = C_a(\delta_a - \delta_{ET})/C_v + \delta_{ET} \quad . \quad (3)$$

For a given time, with various measurements of δ_v and C_v collected at different heights, we are able to estimate the intercept δ_{ET} and slope $k = C_a(\delta_a - \delta_{ET})$ for this moment from regression analysis (Zhang et al., 2011; Wang et al., 2013). Here we focus on the estimation of δ_a using two new methods proposed below.

Intersection point (IP) method. Note that for two nearby time points t_1 and t_2, we could use local constant approximation to estimate δ_a within this time interval since it remains relatively constant over a short period of time. By assuming local constant for C_a and δ_a within this time interval, we have

$$k_1 = C_a(\delta_a - \delta_{ET_1}) \quad , \tag{4}$$

$$k_2 = C_a(\delta_a - \delta_{ET_2}) \quad , \tag{5}$$

where k_i and δ_{ET_i} represent the value at t_i for i=1, 2. From (4) and (5), we can solve δ_a as:

$$\delta_a = \frac{k_1\delta_{ET_2} - k_2\delta_{ET_1}}{k_1 - k_2} \quad . \tag{6}$$

The local constant approximation idea was first described in Yamanaka and Shimizu (2007) as an assumption to quantify the contribution of local ET to total atmospheric vapor.

Intermediate Value Theorem (IVT) method. Denote the slope as $k = C_a(\delta_a - \delta_{ET})$. Since $C_a < C_v = C_a + C_{ET}$, we have $C_a = \frac{k}{(\delta_a - \delta_{ET})} < C_v$. We can rearrange $\frac{k}{(\delta_a - \delta_{ET})} < C_v$ to attain δ_a: $\delta_a < \frac{k}{C_v} + \delta_{ET} = \delta_v$ when $k < 0$, and $\delta_a > \frac{k}{C_v} + \delta_{ET} = \delta_v$ when $k > 0$.

For the smooth function $\delta_{\mathrm{a}}(t)$ defined on the interval $[t_1, t_2]$ with the two time points satisfying $k(t_1)\,k(t_2) < 0$, depending on the sign of the slopes $k(t_1)$ and $k(t_2)$ and the order of $\delta_{v_1} = \delta_{\mathrm{v}}(t_1)$ and $\delta_{v_2} = \delta_{\mathrm{v}}(t_2)$ at the two time points t_1 and t_2, it will correspond to one of the situations in **Fig. 1**. For all of the situations, by the Intermediate Value Theorem, there exists a sub-interval $[t_1', t_2'] \subset [t_1, t_2]$ such that the whole range of $\{\delta_{\mathrm{a}}(t): t \in [t_1', t_2']\}$ is within $[min(\delta_{v_1}, \delta_{v_2}), max(\delta_{v_1}, \delta_{v_2})]$. Proof details of this proposition is shown in the appendix. Thus for the two nearby time points t_1 and t_2 with k_1 and k_2 having different signs, δ_a will be between δ_{v_1} and δ_{v_2}. This provides a prerequisite for estimating the parameter of interest δ_a based on Intermediate Value Theorem, which leads to approximation of δ_a within the time interval between t_1 and t_2 using δ_{v_1} and δ_{v_2}:

$$\delta_a \approx \frac{\delta_{v_1} + \delta_{v_2}}{2} \quad . \tag{7}$$

Using this method, we are able to compute δ_a using data points when the slopes of

Keeling plots change signs between two adjacent time points.

2.2 Field observations

2.2.1 Study site

A field measurement was conducted over a maize field (39 ha) from 1st May 2017 to 30st September 2017 at Shiyanghe Experimental Station of China Agricultural University, located in Wuwei of Gansu Province, northwest China (37°85′N, 102°88′E; altitude 1581m). The region belongs to temperate continental climate and is in the oasis within the Shiyang river basin. The annual mean temperature of the study area is about 8.8℃ with pan evaporation of 2000 mm, annual precipitation of 164.4 mm, mean sunshine duration of 3000 h, and frost-free period of more than 150 d. The local crops are irrigated using groundwater with electrical conductivity of 0.62 dSm^{-1}. The groundwater table is 30-40 m below the surface. Maize was sowed on April and harvested on September 2017, with row spacing of 40 cm and plant spacing of 23 cm. The maize growing stage was divided into seedling stage (April 21st –May 20th), jointing stage (May 21st-July 10th), heading period (July 11th-July 31st), pustulation period (August 1st-August 31st) and mature period (September 1st-September 20th).

2.2.2 Instrument setup and measurement design

A 24-meter flux tower, located in the middle of maize field, was used to measure ET flux and isotopic composition of water vapor at different heights. The field is approximately 600 m long and 240 m wide, with a 10% slope decreasing from southwest to northeast. Five gas traps were installed on the flux tower at heights of 4 m, 8 m, 12 m, 16 m and 20 m, respectively. An iron pillar was placed 20 m away from the flux tower. Three gas traps were installed on the iron pillar, one was close to the canopy, and the other two were 2 m and 3 m above the ground.

Canopy gas trap was adjusted weekly according to the height of maize.

In situ δ_v and C_v collected by the eight gas traps were monitored by a water vapor isotope analyzer (L2130-i, Picarro Inc., Sunnyvale, CA, USA), which was a wavelength scanned cavity ring down spectroscope (WS-CRDS) instrument. Vapor specifications include a measurement range from 1000 to 50000 ppm, the precision is 0.040‰ to 0.25‰ for $\delta^{18}O$ (Zhao et al., 2019). Interfacing with the gas trap and the isotope analyzer, teflon tube was wrapped by thermal insulation cotton to avoid vapor condensation during transmission. The measurement of δ_v and C_v were conducted from May to September, which should have 153 days of data. Forty-nine days among them were complete with 24-hour continuous datasets. There were missing data for either a whole day or several hours of a day for other days due to the maintenance of the analyzer. These 49 days was chosen in our study for data analysis.

2.2.3 Calibration of δ_v and C_v

Our calibration procedure mainly followed the study by Steen-Larsen et al. (2013) with some modifications to fit our specific experimental setup. The water vapor from eight inlets were sampled continuously over a 24-hour-period. Since only one analyzer was used to measure the δ_v and C_v, the values of eight sampling inlets were recorded in turn every 225s in a 30 mins cycle. The switch procedure was automatic. As the analyzer makes a measurement every 0.9-1s, approximately 259-264 values for each inlet was recorded within the cycle. For each 225s measurement period, No. 195 to No. 253 data points were used to avoid memory issue and influence of transient pressure variation. The absolute value of coefficient of variations (|CV|) of δ_v and C_v were no more than 0.016 and 0.002, respectively, which was far below the critical value of 15% (Lovie, 2005). The mean value of the selected data points was regarded as the measured δ_v and C_v in a specific inlet. Measured C_v was used directly as actual C_v, while measured δ_v was calibrated to minimize the influence of isotopic concentration dependence. The C_v in our measurement ranged from 5386 ppm to 30255 ppm. Thus, C_v gradients of 10000 ppm, 20000 ppm and 30000 ppm were selected as calibration concentrations to improve the precision of δ_v.

2.3 Data quality control for δ_a estimation

With a 30-min interval for 49 days, we should in theory produce 2352 δ_a values for both IP method and IVT method. However, because of the precondition of $k_1k_2<0$ required for the IVT method, 166 δ_a values was able to be calculated using the IVT method ($\delta_{a(IVT)}$). δ_a values using the IP method ($\delta_{a(IP)}$) was not restricted by this precondition. Furthermore, a filter ($\delta_{ET}<\delta_v<\delta_a$ or $\delta_{ET}>\delta_v>\delta_a$) was used for both methods because δ_v was a mixture of δ_{ET} and δ_a. Therefore, δ_a values that meet both precondition $k_1k_2<0$ and the condition of $\delta_{ET}<\delta_v<\delta_a$ or $\delta_{ET}>\delta_v>\delta_a$ were considered satisfying the criteria for the IVT method; δ_a values that meet the condition of $\delta_{ET}<\delta_v<\delta_a$ or $\delta_{ET}>\delta_v>\delta_a$ were considered satisfying the criteria for the IP method. In the end, we obtained 1264 and 103 δ_a values using IP and IVT methods, respectively (**Table 1**). Eighty eight time points were overlapped between the $\delta_{a(IP)}$ and $\delta_{a(IVT)}$ based δ_a results. These 88 time points were selected to test the reliability of two methods at point to point scale. During the 49 days, there were 21 days when more than one $\delta_{a(IVT)}$ was attained for each day. These 21 days was also used to investigate the time series of daily scale δ_a variations and other isotopic variations. Further analysis in section 2.4 in the following was made on these 21 days.

2.4 Explanations of δ_a using backward trajectories

To explain the variations of estimated δ_a, air mass backward trajectories were calculated using the Hybrid Single Particle Lagrangian Integrated Trajectory (HYSPLIT) model (Draxler and Hess, 1997; Draxler, 2003; Stein et al., 2015; Kaseke et al., 2018) and meteorological data from the Global Data Assimilation System 0.5 Degree (GDAS0p5) with 0.5°×0.5° spatial resolution and 3-hour time resolution for the 21 days mentioned in section 2.3. Five hundred meters height was selected in the modeling. Each backward trajectory was initialized from the station (37°85′N, 102°88′E) at 12:00 pm (local time), and calculated backward for 72 hours. Eighteen trajectories were computed, except for June 21st, August 18th and September 29th when vertical velocity data were missing. Finally, we used these 18 trajectories represented the vapor origin in the corresponding 18 days.

3. **Results**

3.1 Time series variations of δ_{ET}, δ_v, δ_a and k

Time series of isotopic variations were shown in **Fig. 2**. The δ_v here is the average value of eight heights. The average δ_{ET}, δ_v, $\delta_{a(IP)}$ and $\delta_{a(IVT)}$ were -11.04‰, -13.00‰, -13.60‰ and -13.29‰, respectively in those 21 days when more than one $\delta_{a(IVT)}$ was attained for each day. Daytime (7:00am-7:00pm) average δ_{ET}, δ_v, $\delta_{a(IP)}$ and $\delta_{a(IVT)}$ were -10.73‰, -13.33‰, -14.08‰ and -13.63‰, respectively. While at nighttime (7:00pm-7:00am the next day), average δ_{ET} was lower than that at daytime, which was on the contrary with δ_v, $\delta_{a(IP)}$ and $\delta_{a(IVT)}$. The trend of $\delta_{a(IP)}$ and $\delta_{a(IVT)}$ were similar to δ_v. In majority of circumstances, δ_{ET} is the largest of those four isotopic parameters, except on May 19th, June 4th and June 9th. About 76% of k values were negative, and most positive k values occurred at nighttime (60%). The percentage of positive k values were 33%, 34%, 24%, 34% and 10% in May, June, July, August and September, respectively. Standard deviation were used here to evaluate the constancy among isotopic parameters at daily scale. The standard deviation of δ_{ET}, δ_v, $\delta_{a(IP)}$ and $\delta_{a(IVT)}$ were 6.08‰, 0.91‰, 1.38‰ and 0.59‰, respectively. Therefore, the constancy of δ_a was similar to the constancy of δ_v at daily scale.

3.2 Daily variations of HYSPLIT backward trajectories and δ_a using two methods

The 500 m height water vapor backward trajectories revealed that water vapor was from outside the study regions for ten days **(Fig. 3a)**, and water vapor was from local ET for eight days **(Fig. 3b)**.

As for the IP method, 53.7% of $\delta_{a(IP)}$ values met the criteria, and 49.4% of $\delta_{a(IP)}$ values meeting the criteria were during the daytime (7:00am-7:00pm). The range of $\delta_{a(IP)}$ values meeting the criteria were between -16.79‰ and -12.95‰ for the ten days with external origins **(Fig. 3a)**. The range of $\delta_{a(IP)}$ values meeting the criteria were between -12.77‰ and -9.51‰ for the eight days with local origins **(Fig. 3b)**.

As for the IVT method, only 4.4% of δ_a values met the criteria, and 35.9% of δ_a values meeting the criteria were during the daytime (7:00am-7:00pm). The range of $\delta_{a(IVT)}$ values meeting the criteria were between -16.31‰ and -13.93‰ for the ten days with external origins **(Fig. 3a)**. The range of $\delta_{a(IVT)}$ values meeting the criteria were between -12.67‰ and -9.12‰ for the eight days with local origins **(Fig. 3b)**.

3.3 Linear regression between $\delta_{a(IP)}$ and $\delta_{a(IVT)}$

Method comparison was made at both daily scale **(Fig. 4a)** and point to point scale **(Fig. 4b)**. The 21 days (see method section 2.3) in **Fig. 3a** and **Fig. 3b** were selected to figure out the daily scale relationship between $\delta_{a(IP)}$ and $\delta_{a(IVT)}$. Point to point scale data was based on the 88 point of overlapped $\delta_{a(IP)}$ and $\delta_{a(IVT)}$ (see method section 2.3) among all 49 days, which accounted for 7.0% of δ_a values using IP method and 85.4% of δ_a values using IVT method. Linear regression between $\delta_{a(IP)}$ and $\delta_{a(IVT)}$ was significant at both daily scale and point to point scale. The degree of agreement was less for the daily time scale than point to point scale and the RMES between these two methods at daily scale and point to point scale were 0.618‰ and 0.167‰, respectively.

4. **Discussion**

4.1 The reliability of δ_a estimating methods

The IP method was based on the assumption that the ambient sources were the same between two continuous observation moments. This is a reasonable assumption for short time intervals. For the IVT method, δ_a was derived from δ_v in two continuous moments when their Keeling plot slopes were opposite. The opposite slopes of the Keeling plots were the only requirement. As δ_v was almost constant in two continuously moments, $\delta_{a(IVT)}$ was able to be constrained into a small range. The derivation was supported by the Intermediate Value Theorem. Therefore, both methods of estimating δ_a were theoretically sound.

The δ_a results were also examined by HYSPLIT backward trajectories to identify the different sources of water vapor, which assesses the reliability of both methods indirectly. Based on the trajectory analysis, water vapor in the study area came from westerlies, northern polar region and local recirculation. Water vapor from southwest monsoon and northwest Pacific were not detected in this study. Based on the isotope variation of meteoric water (Fricke et al., 1999), water vapor from westerlies and northern polar was more ^{18}O depleted than local recycled moisture through ET. It was also reported that the water vapor from outside the study regions will lower δ_v values (Ma et al., 2014; Chen et al., 2015). The calculated δ_a values of the ten days with external sources (**Fig. 3a)** based on the IP method and IVT approach were higher than those of eight days with local origin (**Fig 3b**), which was consistent with our expectation. The results indicate that quantifying δ_a using both the IP method and IVT approach was reliable. The reliability of two methods at point to point scale were also supported by the close relationship of δ_a using these two independent methods. Daily time scale result is less reliable than point to point scale.

4.2 The application of δ_a for moisture recycling

When δ_a was estimated, moisture recycling (e.g., $f_{ET,}$ the contribution of ET fluxes to the total water vapor) can be estimated using the following equations with known δ_a, δ_{ET}, $\delta_{v,}$ C_{ET} and C_v:

$$C_{ET} = C_v \bullet \frac{\delta_a - \delta_v}{\delta_a - \delta_{ET}} \quad , \qquad (8)$$

$$f_{ET} = \frac{C_{ET}}{C_v} \quad , \qquad (9)$$

According to Eq. (8) and Eq. (9), f_{ET} was only related to δ_a, δ_v, and δ_{ET}. These three parameters were obtained for relatively small temporal and spatial scales in this study, making it possible to estimate f_{ET} at a tower scale. The f_{ET} estimate will provide a baseline value for rainfall recycling ratio calculations. Previous studies quantified the contribution of recycled vapor to annul or monthly precipitation in river basins using two-element mixture model (Kong et al., 2013) and three-element mixture (Peng et al., 2011). At the watershed scale, recycled vapor rate refers to the contributions of moisture from terrestrial ET to annul or monthly precipitation (Trenberth, 1999). It is a key part of local water cycle and the atmospheric water vapor balance (Seneviratne et al., 2006; Aemisegger et al., 2014). In our study, the role of f_{ET}

to regional vapor is similar to the role of recycled vapor rate to annul or monthly precipitation, but f_{ET} was calculated with fine temporal (e.g., hourly) and spatial (i.e., field scale) scales. At the watershed scale, assumption was made that no isotopic fractionation between transpiration and source water (Flanagan et al., 1991); advected vapor was assumed to be the precipitation vapor of the upwind station (Peng et al., 2011). However, the isotope composition of plant transpired vapor is variable in a day especially under non-steady-state conditions (Farquhar and Cernusak, 2005; Lai et al., 2008; Song et al., 2011). In addition, sometimes it is difficult to select an upwind station without precipitation events. In this study, a field site was selected to calculate the proportion of ET fluxes to total atmospheric vapor and f_{ET} was only related to δ_a, δ_v, and δ_{ET} according to Eq. (8) and Eq. (9). This indicates that f_{ET} calculations is possible for small temporal and spatial scales after estimating δ_a using the methods we proposed.

If we assumed that the parameter δ_v in Eq. (8) is the average δ_v value measured from all the eight heights. f_{ET} in this study was 23.3% and 12.7% in May and September 2017 based on daily $\delta_{a(IP)}$ and daily $\delta_{a(IVT)}$, respectively. It was reported that recycled vapor rate in all Shiyang river basin, oasis region, mountain region and desert region were 23%, 28%, 17% and 15%, respectively (Li, et al., 2016; Zhu, et al., 2019). The f_{ET} based on daily $\delta_{a(IP)}$ in our study was close to these earlier studies. The deviation of f_{ET} based on daily $\delta_{a(IVT)}$ compared with previous studies may be because 64.1% of point to point $\delta_{a(IVT)}$ was observed at nighttime. Normally, ET at nighttime is lower than that of daytime. f_{ET} may be underestimated using daily $\delta_{a(IVT)}$. It could also be inferred that f_{ET} estimation using Eq. (9) may be more reliable using daily $\delta_{a(IP)}$ than daily $\delta_{a(IVT)}$.

4.3 Implications of δ_a

The signature of δ_E and δ_T was first introduced by a hypothetical graph shown on **Fig. 5a** (Moreira et al., 1997). Line 1 and line 2 was idealized Keeling plot with pure T and pure E, and Line 3 was the Keeling plot with mixed T and E. The IVT method in this study provided a general explanation of this figure. As T is a major component of ET in the daytime in non-arid region (Wang et al., 2014), the slope is generally negative. When E dominates ET in an ecosystem, such as in the nighttime in non-arid region or in arid region, the slope should be positive. Mathematically, negative slope is due to $\delta_{ET} < \delta_a$ and positive slope is due to $\delta_{ET} > \delta_a$. It also reflected that IVT method could only be used in non-arid ecosystems to ensure the appearance of transfer plus or minus in Keeling plots' slope. On the contrary, IP method may not be restricted by the type of ecosystems. Yamanaka and Shimizu (2007) used the assumption that δ_a of an area of 219.9 km^2 was represented by the intersection point of two Keeling plot lines in different sites with synchronous measurements and they used the intersection value as an approximate value of δ_a. This study was conducted in a maize field using 30-min interval measurements. The results verified Yamanaka and Shimizu's (2007) assumption in such spatial and temporal scale, and indicate that accurate $\delta_{a(IP)}$ could be estimated from the intersection of two Keeling plots regardless the slope being positive or negative, while the $\delta_{a(IVT)}$ should be restricted in the area between two dotted lines as shown in **Fig. 5b** (i.e., between the minimum value of δ_v in positive slope and the maximum value of δ_v in negative slope). Although IVT method relies on more stringent precondition for data filtering, this method requires a very simple expression, which only need two parameters to be measured according to Eq. (7).

While this study is about water vapor ^{18}O, the "Keeling plot" was first used by (Keeling, 1958, 1961) to interpret carbon isotope ratios of mixed CO_2 and to identify the sources that contribute to increases in atmospheric CO_2 concentrations on a regional basis. Compared with ET in water vapor which consists of E and T, net ecosystem CO_2 exchange is comprised of soil respiration (R) and gross primary productivity (GPP). As $^{13}CO_2$ isotopic Keeling plot reveals a positive slope during both daytime and nighttime (Yakir and Wang, 1996; Unger et al., 2010), the IVT method may not be able to estimate ambient $^{13}CO_2$ isotopic composition ($\delta_a{}^{13}C$) since there are no opposite slopes in a day. In such case, the IP method may be implemented in two continuous moments to estimate $\delta_a{}^{13}C$ and may consequently further calculate the contribution of NEE to atmospheric CO_2.

5. **Conclusions**

In this study, we established two methods to quantify δ_a using intersection point method and the Intermediate Value Theorem method. The IVT method was used under the condition of opposite slope of Keeling plots in two continuously moments. The results of estimated $\delta_{a(IP)}$ and $\delta_{a(IVT)}$ were consistent with the expectation whether it was local origin or external origin using external vapor tracking investigation by HYSPLIT model. The linear regression between $\delta_{a(IP)}$ and $\delta_{a(IVT)}$ was highly significant both on daily time scale and point to point scale.

This study provided insights into the underexplored traditional Keeling plots and provided two methods to estimate δ_a using the same instrumental setup for the traditional Keeling plot investigations. The estimated δ_a will make it possible to calculate the ET contribution to regional vapor at a 30 min interval at field scale. The results indicate that using similar framework, $\delta_a{}^{13}C$ may also solvable by the IP method.

6. Acknowledgements

We acknowledge support from the National Natural Science Foundation of China (51725904, 51621061, 51861125103), the National Key Research Program (2016YFC0400207), the Discipline Innovative Engineering Plan (111 Program, B14002), and the President's International Research Awards from Indiana University and the Division of Earth Sciences of National Science Foundation (EAR-1554894). We thank Dr. Qianning Liu from Jiangxi University of Finance and Economics and Dr. Zhengxiang Chen from Capital Normal University for checking the validity of the Intermediate Value Theorem method.

7. Code and Data availability

Code and data are available on request.

8. Author contribution

YY, TD and LW conceptualized the main research questions. YY collected data and performed the data analyses. YY and LW wrote the first draft. HW contributed to additional data analyses. All the authors contributed ideas and edited the manuscript.

9. Competing interests

There authors declare no competing interests.

10. References

Aemisegger, F., Pfahl, S., Sodemann, H., Lehner, I., Seneviratne, S. I., and Wernli, H.: Deuterium excess as a proxy for continental moisture recycling and plant transpiration, **Atmospheric Chemistry and Physics**, 14, 4029–4054, doi: 10.5194/acp-144029-2014, 2014.

Brunel, J. P., Walker, G. R., Dighton, J. C., and Monteny, B.: Use of stable isotopes of water to determine the origin of water used by the vegetation and to partition evapotranspiration. A case study from HAPEX-Sahel, **Journal of Hydrology**, 188–189, 466–481, doi:10.1016/s0022-1694(96)03188-5, 1997.

Chen, F. L., Zhang, M. J., Ma, Q., Wang, S. J., Li, X. F., and Zhu, X. F.: Stable isotopic characteristics of precipitation in Lanzhou city and its surrounding areas, Northwest China, **Environmental Earth Sciences**, 73, 4671–4680, doi: 10.1007/s12665-014-3776-6, 2015.

Corneo, P. E., Kertesz, M. A., Bakhshandeh, S., Tahaei, H., Barbour, M. M., and Dijkstra, F. A.: Studying root water uptake of wheat genotypes in different soils using water $\delta^{18}O$ stable isotopes, **Agriculture, Ecosystems & Environment**, 264, 119-129, doi: 10.1016/j.agee.2018.05.007, 2018.

Craig, H. and Gordon, L. I.: Deuterium and oxygen 18 variations in the ocean and marine atmosphere, in: **Stable Isotopes in Oceanographic Studies and Paleotemperatures**, p. 9, 1965.

Cui, J., Tian, L., Wei, Z., Huntingford, C., Wang, P., Cai, Z., Ma, N., and Wang, L.: Quantifying the controls on evapotranspiration partitioning in the highest alpine meadow ecosystems, **Water Resources Research**, 56, doi: 10.1029/2019WR024815, 2020.

Draxler, R. R., and Hess, G.: Description of the HYSPLIT4 modeling system, **NOAA Tech Memo ERL ARL-224**, Dec, 24p., 1997.

Draxler, R. R.: Evaluation of an ensemble dispersion calculation, **Journal of Applied Meteorology**, 42, 308-317, doi: 10.1175/1520-0450(2003)042<0308:EOAEDC>2.0.CO;2, 2003.

Farquhar, G. D., and Cernusak, L. A.: On the isotopic composition of leaf water in the non-steady state, **Functional Plant Biology**, 32(4), 293-303, doi: 10.1071/FP04232, 2005.

Fiorella, R. P., Poulsen, C. J., and Matheny, A. M.: Seasonal patterns of water cycling in a deep, continental mountain valley inferred from stable water vapor isotopes, **Journal of Geophysical Research: Atmospheres**, 123, 7271-7291, doi: 10.1029/2017JD028093, 2018.

Flanagan, L. B., Comstock, J. P., and Ehleringer, J. R.: Comparison of modeled and observed environmental influences on the stable oxygen and hydrogen isotope composition of leaf water in Phaseolus vulgaris L, **Plant Physiology**, 96, 588-596, doi: https://doi.org/10.1104/pp.96.2.588, 1991.

Fricke, H. C., O'Neil, J. R. J. E., and Letters, P. S.: The correlation between $^{18}O/^{16}O$ ratios of meteoric water and surface temperature: its use in investigating terrestrial climate change over geologic time, **Earth and Planetary Science Letters**, 170, 181-196, doi: 10.1016/S0012-821X(99)00105-3, 1999.

Galewsky, J., Rella, C., Sharp, Z., Samuels, K., and Ward, D.: Surface measurements of upper tropospheric water vapor isotopic composition on the Chajnantor Plateau, Chile, **Geophysical Research Letters**, 38, 1-5, doi: 10.1029/2011GL048557, 2011.

Good, S. P., Soderberg, K., Wang, L., and Caylor, K. K.: Uncertainties in the assessment of the isotopic composition of surface fluxes: A direct comparison of techniques using laser-based water vapor isotope analyzers, **Journal of Geophysical Research: Atmospheres**, 117, doi: 10.1029/2011JD017168, 2012.

Griffis, T. J., Wood, J. D., Baker, J. M., Lee, X., Xiao, K., Chen, Z., Welp, L. R., Schultz, N. M., Gorski, G., and Chen, M.: Investigating the source, transport, and isotope composition of water vapor in the planetary boundary layer, **Atmospheric Chemistry and Physics**, 16, 5139-5157, doi: 10.5194/acp-16-5139-2016, 2016.

Hobbins, M. T., Ramirez, J. A., and Brown, T. C.: The complementary relationship in estimation of regional evapotranspiration: An enhanced advection-aridity model, **Water Resources Research**, 37, 1389-1403, doi: 10.1029/2000WR900359, 2001.

Jung, M., Reichstein, M., Ciais, P., Seneviratne, S. I., Sheffield, J., Goulden, M. L., Bonan, G., Cescatti, A., Chen, J., and De Jeu, R.: Recent decline in the global land evapotranspiration trend due to limited moisture supply, **Nature**, 467, 951-954, doi: 10.1038/nature09396, 2010.

Kaseke, K. F., Wang, L., Wanke, H., Tian, C., Lanning, M., and Jiao, W.: Precipitation origins and key drivers of precipitation isotope (^{18}O, ^{2}H, and ^{17}O) compositions over windhoek, **Journal of Geophysical Research: Atmospheres**, 123, 7311-7330, doi: 10.1029/2018JD028470, 2018.

Keeling, C. D.: The concentration and isotopic abundances of atmospheric carbon dioxide in rural areas, **Geochimica et Cosmochimica Acta**, 13, 322-334, doi: 10.1016/0016-7037(58)90033-4, 1958.

Keeling, C. D.: The concentration and isotopic abundances of carbon dioxide in rural and marine air, **Geochimica et Cosmochimica Acta**, 24, 277-298, doi: 10.1016/0016-7037(61)90023-0, 1961.

Keppler, F., Schiller, A., Ehehalt, R., Greule, M., Hartmann, J., and Polag, D.: Stable isotope and high precision concentration measurements confirm that all humans produce and exhale methane, **Journal of Breath Research**, 10, 016003, doi: 10.1088/1752-7155/10/1/016003, 2016.

Kerstel, E., and Gianfrani, L.: Advances in laser-based isotope ratio measurements: selected applications, **Applied Physics B**, 92, 439-449, doi: 10.1007/s00340-008-3128-x, 2008.

Kong, Y., Pang, Z., and Froehlich, K.: Quantifying recycled moisture fraction in precipitation of an arid region using deuterium excess, **Tellus B: Chemical and Physical Meteorology**, 65, 19251, doi: 10.3402/tellusb.v65i0.19251, 2013.

Lai, C.T., Ometto, J. P., Berry, J. A., Martinelli, L. A., Domingues, T. F., and Ehleringer, J. R.: Life form-specific variations in leaf water oxygen-18 enrichment in Amazonian vegetation, **Oecologia**, 157, 197-210, doi: 10.1007/s00442-008-1071-5, 2008.

Lanning, M., Wang, L., Benson, M., Zhang, Q., and Novick, K. A.: Canopy isotopic investigation reveals different water uptake dynamics of maples and oaks, **Phytochemistry**, 175, 112389, doi:10.1016/j.phytochem.2020.112389, 2020.

Li, Z., Feng, Q., Wang, Q., Kong, Y., Chen, A., Song, Y., Li, Y., Li, J., and Guo, X.: Contributions of local terrestrial evaporation and transpiration to precipitation using δ^{18}O and D-excess as a proxy in Shiyang inland river basin in China, **Global and Planetary Change**, 146, 140-151, doi: 10.1016/j.gloplacha.2016.10.003, 2016.

Lovie, P.: Coefficient of variation**, Encyclopedia of Statistics in Behavioral Science**, doi: 10.1002/0470013192.bsa107, 2005.

Ma, Q., Zhang, M., Wang, S., Wang, Q., Liu, W., Li, F., and Chen, F.: An investigation of moisture sources and secondary evaporation in Lanzhou, Northwest China, **Environmental Earth Sciences**, 71, 3375-3385, doi: 10.1007/s12665-013-2728-x, 2014.

Mahindawansha, A., Orlowski, N., Kraft, P., Rothfuss, Y., Racela, H., and Breuer, L.: Quantification of plant water uptake by water stable isotopes in rice paddy systems, **Plant and Soil**, 429, 281-302, doi: 10.1007/s11104-018-3693-7, 2018.

Majoube, M.: Fractionnement en oxygene 18 et en deuterium entre l'eau et sa vapeur, **Journal de Chimie Physique**, 68, 1423-1436, doi: 10.1051/jcp/1971681423, 1971.

Merlivat, L., and Jouzel, J.: Global climatic interpretation of the deuterium-oxygen 18 relationship for precipitation, **Journal of Geophysical Research: Oceans**, 84, 5029-5033, doi: 10.1029/JC084iC08p05029, 1979.

Miller, J. B., and Tans, P. P.: Calculating isotopic fractionation from atmospheric measurements at various scales, **Tellus B**, 55, 207-214, doi: 10.1034/j.1600-0889.2003.00020.x, 2003.

Moreira, M., Sternberg, L., Martinelli, L., Victoria, R., Barbosa, E., Bonates, L., and Nepstad, D.: Contribution of transpiration to forest ambient vapour based on isotopic measurements, **Global Change Biology**, 3, 439-450, doi: 10.1046/j.1365-2486.1997.00082.x, 1997.

Parkes, S., McCabe, M., Griffiths, A. D., Wang, L., Chambers, S., Ershadi, A., Williams, A. G., Strauss, J., and Element, A.: Response of water vapour D-excess to land-atmosphere interactions in a semi-arid environment, **Hydrolgy and Earth System Sciences**, 21, 533–548, doi:10.5194/hess-21-533-2017, 2016.

Peng, T. R., Liu, K. K., Wang, C. H., and Chuang, K. H.: A water isotope approach to assessing moisture recycling in the island-based precipitation of Taiwan: A case study in the western Pacific, **Water Resources Research**, 47, W08507, doi: 10.1029/2010WR009890, 2011.

Seneviratne, S. I., Lüthi, D., Litschi, M., and Schär, C.: Land–atmosphere coupling and climate change in Europe, **Nature**, 443, 205-209, doi: 10.1038/nature05095, 2006.

Song, X., Barbour, M. M., Saurer, M., and Helliker, B. R.: Examining the large-scale convergence of photosynthesis-weighted tree leaf temperatures through stable oxygen isotope analysis of multiple data sets, **New Phytologist**, 192: 912–924, doi: 10.1111/j.1469-8137.2011.03851.x, 2011.

Song, X., Simonin, K. A., Loucos, K. E., and Barbour, M. M.: Modelling non-steady-state isotope enrichment of leaf water in a gas-exchange cuvette environment, **Plant, Cell & Environment**, 38, 2618-2628, doi: 10.1111/pce.12571, 2015.

Steen-Larsen, H. C., Johnsen, S. J., Masson-Delmotte, V., Stenni, B., Risi, C., Sodemann, H., Balslev-Clausen, D., Blunier, T., Dahl-Jensen, D., and Ellehøj, M. D.: Continuous monitoring of summer surface water vapor isotopic composition above the Greenland Ice Sheet, **Atmospheric Chemistry and Physics**, 13, 4815-4828, doi:10.5194/acp-13-4815-2013, 2013.

Stein, A., Draxler, R. R., Rolph, G. D., Stunder, B. J., Cohen, M., and Ngan, F.: NOAA's HYSPLIT atmospheric transport and dispersion modeling system, **Bulletin of the American Meteorological Society**, 96, 2059-2077, doi: 10.1175/BAMS-D-14-00110.1, 2015.

Trenberth, K. E.: Atmospheric moisture recycling: Role of advection and local evaporation, **Journal of Climate**, 12, 1368-1381, doi: 10.1175/15200442(1999)012<1368:AMRROA>2.0.CO;2, 1999.

Unger, S., Máguas, C., Pereira, J. S., Aires, L. M., David, T. S., and Werner, C.: Disentangling drought-induced variation in ecosystem and soil respiration using stable carbon isotopes, **Oecologia**, 163, 1043-1057, doi: 10.1007/s00442-010-1576-6, 2010.

Wagle, P., Skaggs, T. H., Gowda, P. H., Northup, B. K., and Neel, J. P.: Flux variance similarity-based partitioning of evapotranspiration over a rainfed alfalfa field using high frequency eddy covariance data, **Agricultural and Forest Meteorology**, 285, 107907, doi: 10.1016/j.agrformet.2020.107907, 2020.

Wang, L., Caylor, K. K., and Dragoni, D.: On the calibration of continuous, high-precision $\delta^{18}O$ and $\delta^{2}H$ measurements using an off-axis integrated cavity output spectrometer, **Rapid Communications in Mass Spectrometry**, 23, 530-536, doi: 10.1002/rcm.3905, 2009.

Wang, L., Caylor, K. K., Villegas, J. C., Barron-Gafford, G. A., Breshears, D. D., and Huxman, T. E.: Partitioning evapotranspiration across gradients of woody plant cover: Assessment of a

stable isotope technique, **Geophysical Research Letters**, 37, L09401, doi: 10.1029/2010GL043228, 2010.
Wang, L., Good, S. P., Caylor, K. K., and Cernusak, L. A.: Direct quantification of leaf transpiration isotopic composition, **Agricultural and Forest Meteorology**, 154-155, 127-135, doi: 10.1016/j.agrformet.2011.10.018, 2012.
Wang, L., Niu, S., Good, S. P., Soderberg, K., McCabe, M. F., Sherry, R. A., Luo, Y., Zhou, X., Xia, J., and Caylor, K. K.: The effect of warming on grassland evapotranspiration partitioning using laser-based isotope monitoring techniques, **Geochimica et Cosmochimica Acta**, 111, 28-38, doi: 10.1016/j.gca.2012.12.047, 2013.
Wang, L., Good, S. P., and Caylor, K. K.: Global synthesis of vegetation control on evapotranspiration partitioning, **Geophysical Research Letters**, 41, 6753–6757, 10.1002/2014GL061439, 2014.
Wei, Z., Yoshimura, K., Okazaki, A., Kim, W., Liu, Z., and Yokoi, M.: Partitioning of evapotranspiration using high-frequency water vapor isotopic measurement over a rice paddy field, **Water Resources Research**, 51, 3716-3729, doi: 10.1002/2014WR016737, 2015.
Werner, M., Langebroek, P. M., Carlsen, T., Herold, M., and Lohmann, G.: Stable water isotopes in the ECHAM5 general circulation model: Toward high-resolution isotope modeling on a global scale, **Journal of Geophysical Research: Atmospheres**, 116, D15109, doi:10.1029/2011JD015681, 2011.
Yakir, D., and Wang, X.F.: Fluxes of CO_2 and water between terrestrial vegetation and the atmosphere estimated from isotope measurements, **Nature**, 380, 515-517, doi: 10.1038/380515a0, 1996.
Yakir, D., and Sternberg, L.: The use of stable isotopes to study ecosystem gas exchange, **Oecologia**, 123, 297-311, doi: 10.1007/s004420051016, 2000.
Yamanaka, T., and Shimizu, R.: Spatial distribution of deuterium in atmospheric water vapor: Diagnosing sources and the mixing of atmospheric moisture, **Geochimica et Cosmochimica Acta**, 71, 3162-3169, doi: 10.1016/j.gca.2007.04.014, 2007.
Yepez, E. A., Williams, D. G., Scott, R. L., and Lin, G.: Partitioning overstory and understory evapotranspiration in a semiarid savanna woodland from the isotopic composition of water vapor, **Agricultural and Forest Meteorology**, 119, 53-68, doi: 10.1016/S0168-1923(03)00116-3, 2003.
Zhang, L., Dawes, W., and Walker, G.: Response of mean annual evapotranspiration to vegetation changes at catchment scale, **Water Resources Research**, 37, 701-708, doi: 10.1029/2000WR900325, 2001.
Zhang, Y., Shen, Y., Sun, H., and Gates, J. B.: Evapotranspiration and its partitioning in an irrigated winter wheat field: A combined isotopic and micrometeorologic approach, **Journal of Hydrology**, 408, 203-211, doi: 10.1016/j.jhydrol.2011.07.036, 2011.
Zhao, L., Liu, X., Wang, N., Kong, Y., Song, Y., He, Z., Liu, Q., and Wang, L.: Contribution of recycled moisture to local precipitation in the inland Heihe River Basin, **Agricultural and Forest Meteorology**, 271, 316-335, doi: 10.1016/j.agrformet.2019.03.014, 2019.
Zhu, G., Guo, H., Qin, D., Pan, H., Zhang, Y., Jia, W., and Ma, X.: Contribution of recycled moisture to precipitation in the monsoon marginal zone: Estimate based on stable isotope data, **Journal of Hydrology**, 569, 423-435, doi: 10.1016/j.jhydrol.2018.12.014, 2019.

11. Appendix

Proposition. In the traditional linear Keeling plot system, denote $\delta_a = f(t)$, $\delta_v = g(t)$, $\delta_{ET} = h(t)$ and $C_a = I(t) > 0$ as continuous functions of time. And for two definite moments t_1 and t_2 ($t_1 < t_2$), $\delta_{a_1} \neq \delta_{a_2} \neq \delta_{v_1} \neq \delta_{v_2} \neq \delta_{ET_1} \neq \delta_{ET_2}$. The slopes of corresponding keeling plot curve are $k_1 = C_{a_1}(\delta_{a_1} - \delta_{ET_1})$ and $k_2 = C_{a_2}(\delta_{a_2} - \delta_{ET_2})$, respectively. Then we have that when $k_1 k_2 < 0$, there exists$[t_1{'}, t_2{'}] \subset [t_1, t_2]$, such that $[min(f(t_1{'}), f(t_2{'})), max(f(t_1{'}), f(t_2{'}))] \subset [min(\delta_{v_1}, \delta_{v_2}), max(\delta_{v_1}, \delta_{v_2})]$.

Remark: To make a proof of the proposition, classical Intermediate Value Theorem (IVT) was used. It states that if f is a continuous function from the interval $I = [a, b]$ to real number (R). Then *Version I.* if u is a number between$f(a)$ and$f(b)$, there is *c* in (a, b) such that $f(c) = u$. *Version II.* the image set $f(I)$ is also an interval, and it contains $[min(f(a), f(b)), max(f(a), f(b))]$. While in this study, IVT was able to be explained as follows: if f is a continuous function from the interval $I = [t_1, t_2]$ to R with $min[f(t_1), f(t_2)] < \delta_v$ and $max[f(t_1), f(t_2)] > \delta_v$, then *Version I* implies that there is $t' \in (t_1, t_2)$ such that $f(t') = \delta_v$. And *Version II* implies that the image set $f(I)$ is also an interval, and it contains $[min(f(t_1), f(t_2)), max(f(t_1), f(t_2))]$.

Proof. Since $k_1 k_2 < 0$, we have $\delta_{a_1} < \delta_{v_1}$and $\delta_{a_2} > \delta_{v_2}$, or $\delta_{a_1} > \delta_{v_1}$and $\delta_{a_2} < \delta_{v_2}$. As a result, the cases $\delta_{a_1} < \delta_{v_1} < \delta_{a_2} < \delta_{v_2}$, $\delta_{v_1} < \delta_{a_1} < \delta_{v_2} < \delta_{a_2}$, $\delta_{v_2} < \delta_{a_2} < \delta_{v_1} < \delta_{a_1}$, $\delta_{a_2} < \delta_{v_2} < \delta_{a_1} < \delta_{v_1}$ and $[min(\delta_{v_1}, \delta_{v_2}), max(\delta_{v_1}, \delta_{v_2})] \cap [min(\delta_{a_1}, \delta_{a_2}), max(\delta_{a_1}, \delta_{a_2})] = \emptyset$ do not meet the precondition $k_1 k_2 < 0$. There are only four cases below. We will prove the proposition in each of the four cases.

Case 1: $[min(\delta_{v_1}, \delta_{v_2}), max(\delta_{v_1}, \delta_{v_2})] \subset [min(\delta_{a_1}, \delta_{a_2}), max(\delta_{a_1}, \delta_{a_2})]$ **(Fig. 1 a)**.

According to IVT *Version I*, there exists t_1' $\in [t_1, t_2]$, such that $f(t_1') = \delta_{v_1}$; similarly, there exists t_2' $\in [t_1, t_2]$, such that $f(t_2') = \delta_{v_2}$. Based on IVT *Version II*, there exists $\left[t_1', t_2'\right] \subset [t_1, t_2]$, such that $[min(f(t_1'), f(t_2')), max(f(t_1'), f(t_2'))] = [min(\delta_{v_1}, \delta_{v_2}), max(\delta_{v_1}, \delta_{v_2})]$.

Case 2: $[min(\delta_{a_1}, \delta_{a_2}), max(\delta_{a_1}, \delta_{a_2})] \subset [min(\delta_{v_1}, \delta_{v_2}), max(\delta_{v_1}, \delta_{v_2})]$ **(Fig. 1 b)**.

According to IVT *Version I*, there exists t_1' $\in [t_1, t_2]$, such that $f(t_1') = \delta_{a_1}$; similarly, there exists t_2' $\in [t_1, t_2]$, such that $f(t_2') = \delta_{a_2}$. Based on IVT *Version II*, there exists $\left[t_1', t_2'\right] \subset [t_1, t_2]$, such that $[min(f(t_1'), f(t_2')), max(f(t_1'), f(t_2'))] = [min(\delta_{a_1}, \delta_{a_2}), max(\delta_{a_1}, \delta_{a_2})] \subset [min(\delta_{v_1}, \delta_{v_2}), max(\delta_{v_1}, \delta_{v_2})]$.

Case 3: $\delta_{v_2} < \delta_{a_1} < \delta_{v_1} < \delta_{a_2}$, or $\delta_{a_2} < \delta_{v_1} < \delta_{a_1} < \delta_{v_2}$ **(Fig. 1 c and Fig. 1 d)**.

According to IVT Version I, there exists t_2' $\in [t_1, t_2]$, such that $f(t_2') = \delta_{v_1}$. Given case (2), when $[\min(\delta_{a_1}, \delta_{v_1}), \max(\delta_{a_1}, \delta_{v_1})] \subset [min(\delta_{v_1}, \delta_{v_2}), max(\delta_{v_1}, \delta_{v_2})]$, there exists $\left[t_1', t_2'\right] \subset \left[t_1, t_2'\right] \subset [t_1, t_2]$, such that $[min(f(t_1'), f(t_2')), max(f(t_1'), f(t_2'))] \subset [min(\delta_{a_1}, \delta_{v_1}), max(\delta_{a_1}, \delta_{v_1})] \subset [min(\delta_{v_1}, \delta_{v_2}), max(\delta_{v_1}, \delta_{v_2})]$.

Case 4: $\delta_{v_1} < \delta_{a_2} < \delta_{v_2} < \delta_{a_1}$, or $\delta_{a_1} < \delta_{v_2} < \delta_{a_2} < \delta_{v_1}$ **(Fig. 1 e and Fig.1 f)**.

According to IVT Version I, there exists t_1' $\in [t_1, t_2]$, such that $f(t_1') = \delta_{v_2}$. Based on case (2), when $[\min(\delta_{a_2}, \delta_{v_2}), \max(\delta_{a_2}, \delta_{v_2})] \subset [min(\delta_{v_1}, \delta_{v_2}), max(\delta_{v_1}, \delta_{v_2})]$, there exists $\left[t_1', t_2'\right] \subset \left[t_1', t_2\right] \subset [t_1, t_2]$, such that $[min(f(t_1'), f(t_2')), max(f(t_1'), f(t_2'))] \subset [min(\delta_{a_2}, \delta_{v_2}), max(\delta_{a_2}, \delta_{v_2})] \subset [min(\delta_{v_1}, \delta_{v_2}), max(\delta_{v_1}, \delta_{v_2})]$.

Thus the proposition is true for all four possible scenarios, which make the estimation of δ_a theoretically feasibly when $k_1 k_2 < 0$ and δ_{v_1} and δ_{v_2} adequately close. Actual δ_a between t_1 and t_2 can be ensured in the interval $[min(\delta_{v_1}, \delta_{v_2}), max(\delta_{v_1}, \delta_{v_2})]$.

To simplify the result, actual δ_a between t_1 and t_2 can be approximately regarded as what Eq. (7) reveals.

Table 1. The number of estimated isotope composition of ambient vapor meeting the criteria using the intersection point method ($\delta_{a(IP)}$) and the Intermediate Value Theorem method ($\delta_{a(IVT)}$) among all 49 days.

Date	number of $\delta_{a\ (IP)}$ values meeting the criteria in a whole day	number of $\delta_{a\ (IVT)}$ values meeting the criteria in a whole day
5/19	27	8
5/27	13	3
5/28	30	3
5/31	25	5
6/4	38	5
6/5	28	0
6/7	29	6
6/9	32	5
6/10	26	2
6/11	21	4
6/12	22	4
6/15	32	0
6/16	33	0
6/17	24	1
6/18	26	0
6/21	26	3
6/22	22	0
6/26	22	0
6/27	29	3
7/4	23	0
7/5	23	1
7/7	30	0
7/8	29	0
7/14	28	4
7/16	28	0
7/18	25	1
7/19	28	6
7/20	27	6
7/21	29	0
7/22	19	0
8/3	18	1
8/4	22	3
8/5	25	3
8/6	28	1
8/12	13	8
8/18	19	3
8/19	30	0
8/28	23	0
8/29	22	1
8/30	27	1
8/31	27	0
9/20	25	0
9/21	24	1
9/22	31	1
9/23	28	1
9/27	28	2
9/28	25	1
9/29	30	5
9/30	25	1

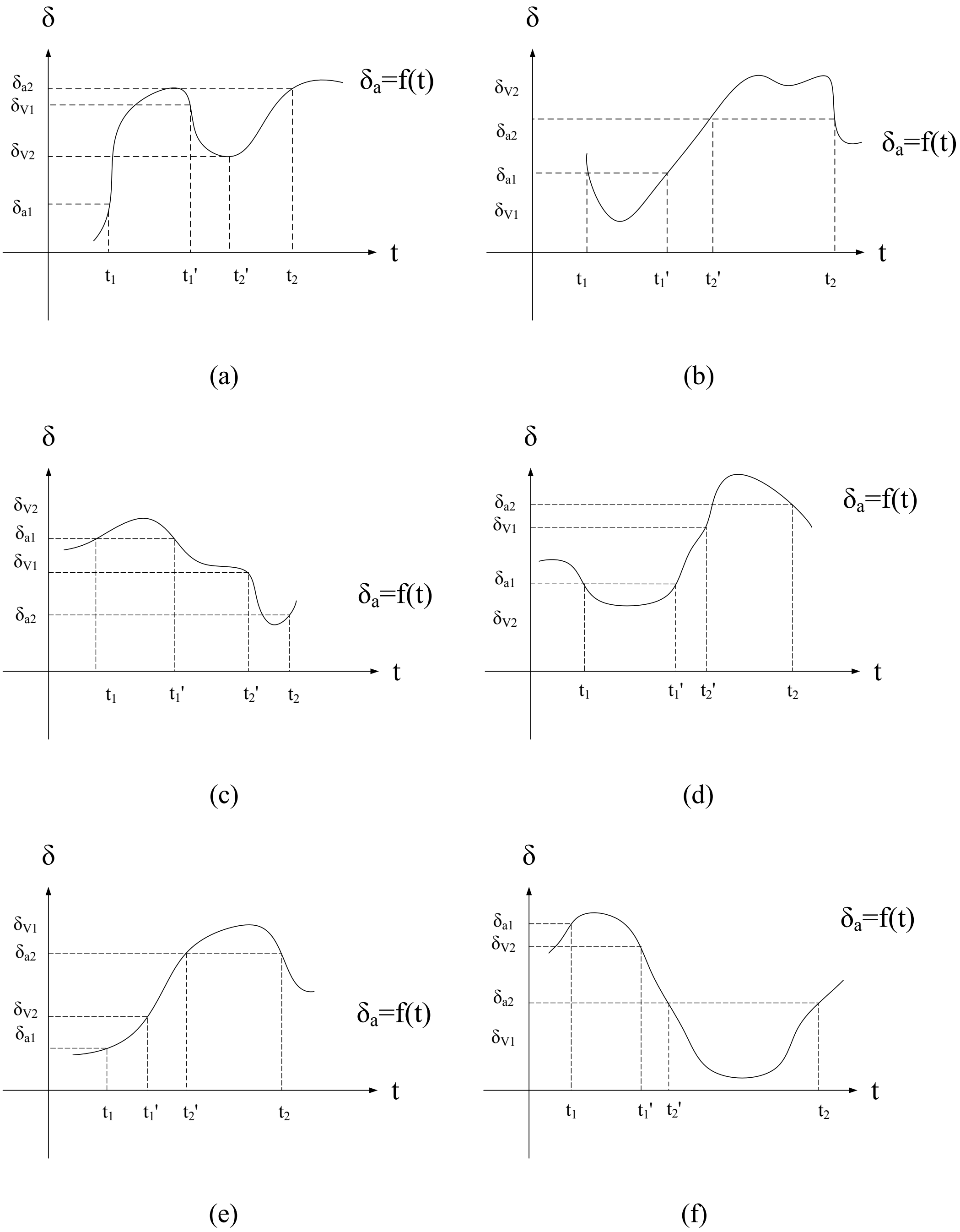

Fig. 1 Theoretical diagrams of all possible combinations of the relationships between isotope composition of ambient vapor (δ_a) and observed isotope composition of atmospheric vapor (δ_v) of two continuous moments t_1 and t_2, ($t_1 < t_2$). δ_{a1} and δ_{a2} represent δ_a value in t_1 and t_2, respectively. δ_{v1} and δ_{v2} represent δ_v value in t_1 and t_2, respectively. t_1' and t_2' represent the time of two specific moments between t_1 and t_2 with $t_1 < t_1' < t_2' < t_2$. For all of the six situations, there exists some sub-intervals $[t_1', t_2'] \subset [t_1, t_2]$ such that the whole range of $\{\delta_a(t): t \in [t_1', t_2']\}$ is within $[min(\delta_{v_1}, \delta_{v_2}), max(\delta_{v_1}, \delta_{v_2})]$.

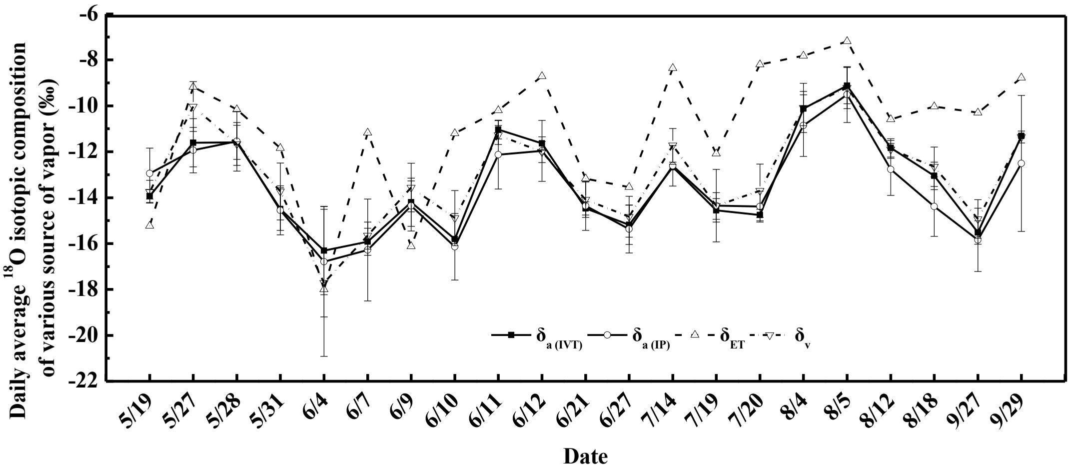

Fig. 2 The daily average values of the isotope composition of evapotranspiration vapor (δ_{ET}), the isotope composition of atmospheric vapor (δ_v), the estimated isotope composition of ambient vapor using the intersection point method ($\delta_{a(IP)}$) and the Intermediate Value Theorem method ($\delta_{a(IVT)}$) in the 21 days (see method section 2.3).

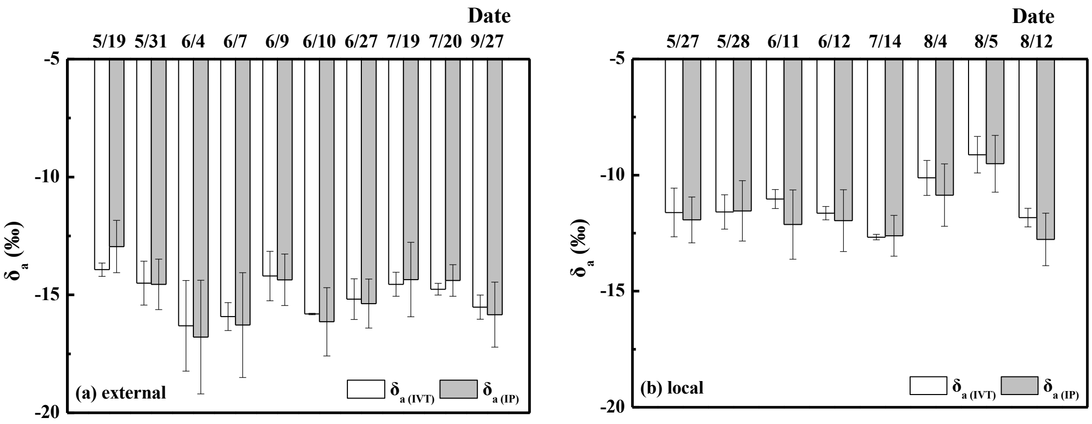

Fig. 3 The daily average values of the estimated isotope composition of ambient vapor using the intersection point method ($\delta_{a(IP)}$) and the Intermediate Value Theorem method ($\delta_{a(IVT)}$) after filter. Hybrid Single Particle Lagrangian Integrated Trajectory (HYSPLIT) backward trajectory showed external origin (a) and local origin (b), respectively.

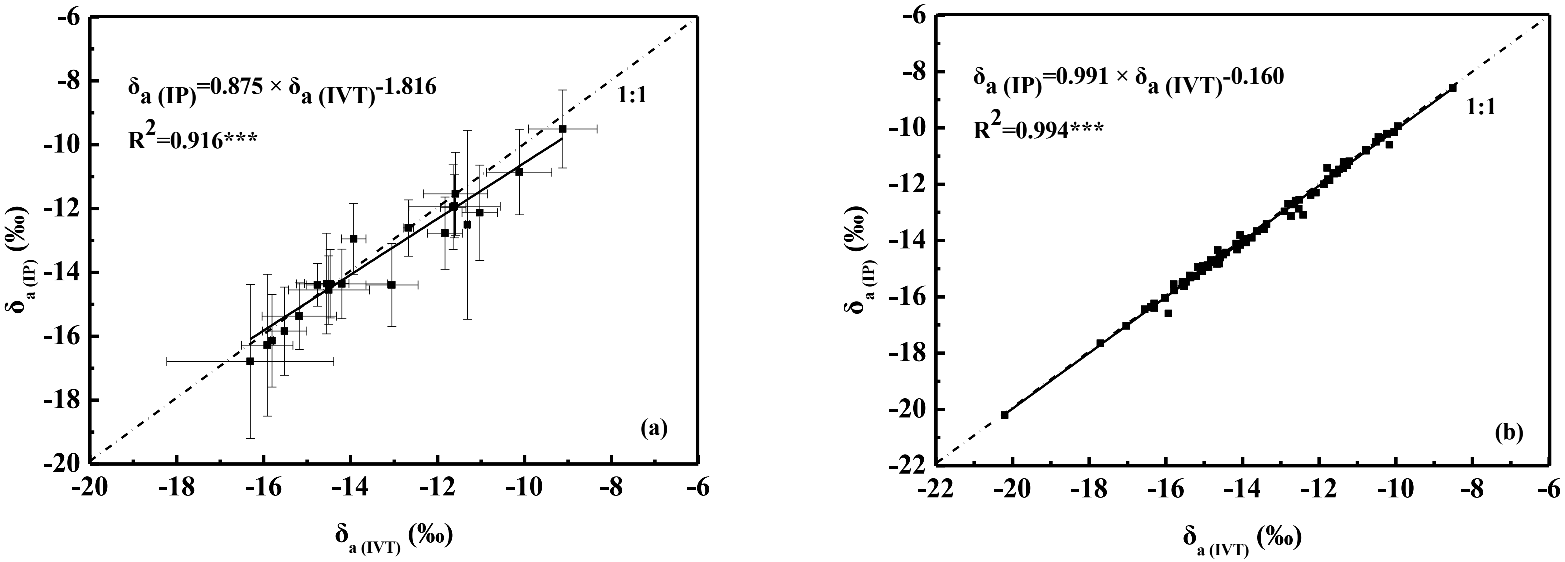

Fig. 4 Linear regression between the estimated isotope composition of ambient vapor using the intersection point method ($\delta_{a(IP)}$) and the Intermediate Value Theorem method ($\delta_{a(IVT)}$) on daily scale (a) and point to point scale (b), respectively.

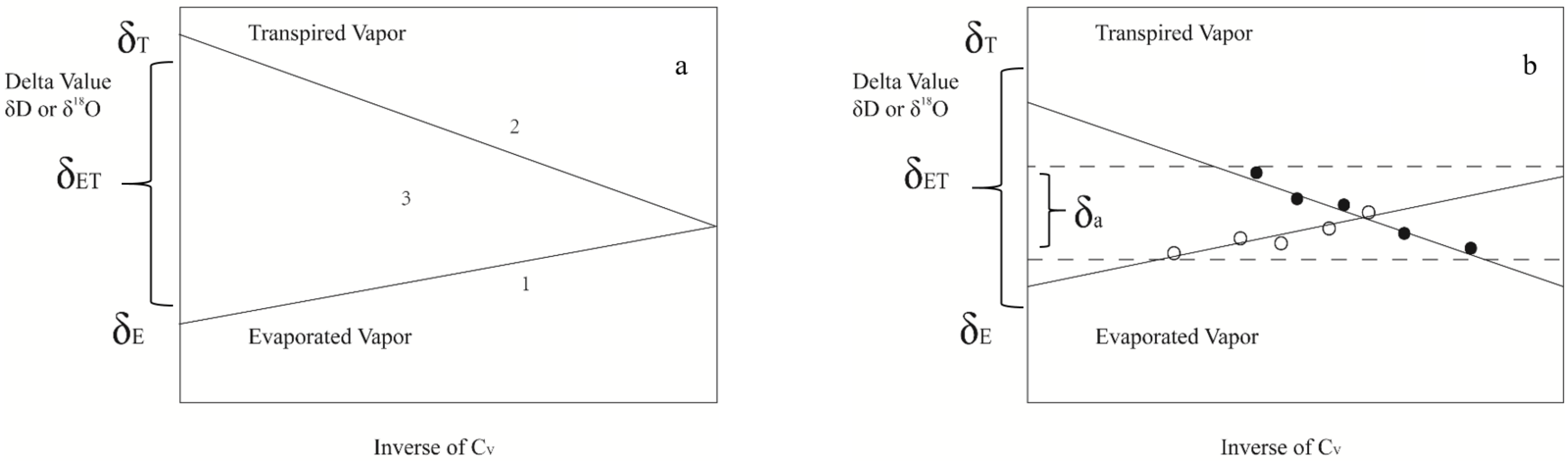

Fig. 5 Hypothetical graph of the idealized Keeling plot curve of the isotope composition of evaporation vapor (δ_E) curve (line 1), the isotope composition of transpiration vapor (δ_T) curve (line 2) and the isotope composition of evapotranspiration vapor (δ_{ET}) curve (area 3) (a), and hypothetical graph of idealized δ_E, δ_T lines and the interval of possible the isotope composition of ambient vapor (δ_a) in the Keeling plots (b).